Electronic structure and stability of a model of the decagonal quasicrystal Al-Cu-Co

1995 J. Phys.: Condens. Matter 7 5437

(http://iopscience.iop.org/0953-8984/7/28/004)

J. Phys.: Condens. Matter 7 (1995) 5437–5459. Printed in the UK

Electronic structure and stability of a model of the decagonal quasicrystal Al–Cu–Co

R F Sabiryanov†, S K Bose† and S E Burkov‡

† Department of Physics, Brock University, St Catharines, Ontario, Canada L2S 3A1

‡ Department of Physics, University of Wisconsin, Madison, WI 53706, USA

Received 29 July 1994, in final form 19 April 1995

Abstract. We present an electronic structure study of a model of the decagonal quasicrystal Al–Cu–Co, proposed by one of us (SEB). Both quasicrystalline clusters and their crystalline counterparts are examined. The locations and the ratio of the concentrations of Cu and Co atoms in the model are found to be important in determining the shape and the magnitude of the density of states at the Fermi level. A local minimum in the density of states (DOS) at the Fermi level is exhibited only by clusters with a Cu concentration larger than Co. However, such clusters do not have the lowest internal (band) energy. No DOS minimum at the Fermi level is obtained for clusters with equal or nearly equal Cu and Co concentrations. Spectral functions reveal no evidence of a pseudogap originating from a Fermi-surface–Jones-zone-boundary interaction. Eigenstates at the Fermi level do not appear localized within the clusters used in our calculations.

1. Introduction

Thermodynamically stable decagonal quasicrystals Al–Cu–Co and Al-Ni–Co have been the subject of considerable recent interest. Experimental results [1] on structural [2–8] as well as thermal [9] and electrical [10] transport properties on these alloys are now available. Burkov [11] has presented a structural model for Al–Cu–Co (previously thought to be isostructural to Al–Ni–Co), in fair agreement with the available x-ray diffraction [7] and high-resolution electron microscopy (HREM) [5] results. According to a comparison of the various models available for Al–transition metal decagonal quasicrystals by Henley [12] this model is the best from the viewpoint of high-density packing without close pairs. The stability of this model has been examined by Phillips and Widom [13], using pseudopotential-based pair interactions. Recently Trambly de Laissardiere and Fujiwara [14] have studied the electronic structure of crystalline approximants based on this model. To date most electronic structure calculations for quasicrystals have been limited to the icosahedral phase [15–17], and its rational approximants. One common feature emerging from these calculations is a pseudogap (a pronounced local minimum in the density of states) at the Fermi level, E_F. The origin of this pseudogap is believed to be a Hume–Rothery-like Fermi-surface–pseudo-Jones-zone-boundary (FS–JZB) interaction [18]. The pseudogap at the Fermi level lowers the electronic energy and is deemed to be an important factor in stabilizing the icosahedral quasicrystalline phase. This is reminiscent of the Nagel–Tauc [19] criterion for the stability of metallic glasses.

The Burkov [11] model agrees to a large extent with a three- and five-dimensional Patterson analysis of x-ray diffraction data and with direct-space atomic patterns found by high-resolution electron microscopy. However, experiments so far have not been able to distinguish between the locations of the Cu and Co atoms. Thus the model distinguishes

0953-8984/95/285437+23$19.50

only between the positions of the Al and the transition metal (TM) atoms (both Cu and Co being considered as TM).

The object of the present paper is to study how the locations and the concentrations of Cu and Co atoms in the model influence the internal energy and the shape and magnitude of the DOS at E_F. Changing the positions of the Cu and Co atoms results in a change of their relative concentrations, while the Al concentration remains fixed at a value $\tau - 1$ $(= \tau^{-1})$, where τ is the golden mean. We wish to explore whether a pseudogap due to FS–JZB exists in the Burkov model. Recent experimental works on decagonal Al–Cu–Co and Al–Ni–Co quasicrystals [10, 20a] report negatively on the existence of a pseudogap. Basov and co-workers [10] have carried out optical and far-infrared conductivity measurements on high-quality decagonal $Al_{65}Co_{17}Cu_{18}$ and $Al_{62}Co_{15}Cu_{20}Si_3$ samples. From an analysis of their results they conclude that the pseudogap in these systems, if present at all, must be far less developed than in icosahedral quasicrystals. Stadnik and co-workers [20a] have carried out photoemission spectroscopy on high-quality decagonal $Al_{65}Co_{15}Cu_{20}$ and $Al_{70}Co_{15}Ni_{15}$ alloys to determine the valence bands and find no evidence of a pseudogap in these systems. It is important to mention that similar measurements by Stadnik and co-workers [20b] on icosahedral quasicrystals show a pseudogap or gap at the Fermi level. Measurements of transport properties by Basov and co-workers [10] on decagonal Al–Cu–Co samples also reveal remarkable anisotropy: electrical resistivity along the quasiperiodic plane is roughly 15 times higher than that along the c axis. The enhanced resistivity in the quasiperiodic plane could be due to increased scattering or some kind of weak localization. To shed some light on this question we have examined the localization of states in this model.

We have studied, in total, six structures. All of these reflect possible variations of the Burkov model. Two of these structures are not consistent with diffraction results. However, even these structures are worth studying. To quote from a recent article by Henley [12], all well packed models are worthy of study even when they contradict known experiments, since a proper theory of the origin of decagonals must explain not only the existence of the observed structures, but the non-existence of the unobserved ones.

The electronic structure of the model is studied using the tight-binding linear muffin-tin orbitals (TB-LMTO) basis [21a] and the recursion method [22]. In addition to the quasicrystalline phase, we have considered its crystalline counterpart, the thermodynamically stable crystalline alloy $Al_{60}Cu_{30}Co_{10}$ [23]. By examining the spectral function for the quasicrystalline clusters, we obtain the (quasi)band structure along various symmetry directions in the quasiperiodic reciprocal plane as well as the periodic tenfold symmetry axis perpendicular to this plane. The localization of the eigenstates at the Fermi level is studied by calculating the generalized participation ratio [24], or the 2p-(pseudo)norm discussed by Tsunetsugu and co-workers [25].

The remainder of this paper is organized as follows. In section 2 we discuss some features of the Burkov model [11] that are relevant to our electronic structure calculation. In section 3 we present the electronic structures of various clusters with different concentrations and locations of the TM atoms in the Burkov model, and discuss the stability in the light of our electronic structure calculation. In section 4 we present the spectral functions, and discuss their relevance to the study of electrical conduction properties, as well as the possibility of (quasi)band gaps as a result of the Fermi-surface–pseudo-Jones-zone-boundary (FS–JZB) interaction. In section 5 we present the results of our localization study for various clusters. In section 6 we present a summary of our results.

2. Burkov model for the decagonal quasicrystal Al–Cu–Co

Decagonal quasicrystals have a layered structure, with every layer being a two-dimensional quasicrystal. The stacking of layers along the tenfold (z) axis is periodic. In the Burkov model there are two plane layers per vertical period ($c = 4.08$ Å). Each layer has only a fivefold symmetry, but the layer at $z = c/2$ is rotated 36° with respect to the layer at $z = 0$, revealing overall decagonal symmetry. The smallest interplane as well as intraplane interatomic distance is 2.44 Å. In figure 1(a) we show the latest version of the model [11a]. The model views the structure as consisting of two decagonal clusters, small and large. In the present work we will refer to them as small and large atomic motifs (SAM and LAM). In the original version [11b] the structure was viewed as a binary tiling with two Penrose rhombuses, with the tiling sites being occupied by these two types of cluster, or motif. In the latest version [11a] the tiling is viewed as the Klotz triangle tiling [26], with only the LAM sitting at the tiling sites. In the original Burkov model when two large decagons (peripheries of LAM) touched, their outer rings shared an unphysically short Al–Al bond of length 1.77 Å. These atoms have been moved using the pseudopotential-based pair interaction of Phillips and Widom [13]. The pseudopotential used by Phillips and Widom [13] is not accurate enough to yield the best possible Al–Al equilibrium distance. However, the Al atoms that are relaxed using this pseudopotential constitute only 5% of the total number of Al atoms (10 out of a 198-atom cluster in figure 1(a)), and the fact that these Al atoms are not at their optimum location should not drastically affect the electronic properties of the model. In figure 1(a) the Al atoms are shown as circles, the Cu atoms as triangles and Co atoms as rectangles: empty symbols mark the $z = 0$ layer and full symbols the $z = c/2$ layer. The large circle (not the LAM) centred at the origin of the cluster shows the boundary of the 198-atom (in a single plane) cluster used in our TB-LMTO recursion calculations (section 3). Figure 1(b) shows the symmetry directions along which we have calculated the spectral functions (section 4).

Since the experiments have not been able to distinguish between the Cu and Co atoms, there are various possible choices in the Burkov model for the positions as well as relative concentrations of Cu and Co atoms, all of which should be consistent with the available experimental data. Future experiments may further narrow, or eliminate, this choice. In the absence of experimental data several theoretical speculative models were proposed. These theoretical suggestions are no more than hypotheses, in contrast with allocating Al and TM atoms, which could be classified as deciphering real quasicrystalline structures. One such proposed cluster, which we will call the Burkov cluster, was introduced in [11a] as a mere illustration of how certain abstract mathematical concepts of Baake and co-workers [26] *might* be enforced in real quasiperiodic alloys. This model results in a concentration $\tau' = (2 - \tau)/2$ for Cu and Co atoms.

We have calculated the electronic structure of the Burkov model as presented in figure 1(a) [11a], as well as its various modifications. One such modification, suggested by Phillips and Widom [13], consists of interchanging the two inner rings in the LAM. This change moves the Al atoms from the second ring, as in [11], into the innermost ring of the LAM. Phillips and Widom, based on their pseudopotentials, showed that this change results in a lowering of the energy. In the next section we present the electronic structures for the Burkov model of figure 1(a), and the model with the ring interchange suggested by Phillips and Widom [13]. The latter will be referred to as cluster 1. We also consider various other modifications in the locations and concentrations of TM atoms. In table 1 we present five chosen modifications in terms of locations and concentrations of Cu and Co atoms. These modifications are natural choices from the viewpoint of symmetry. There

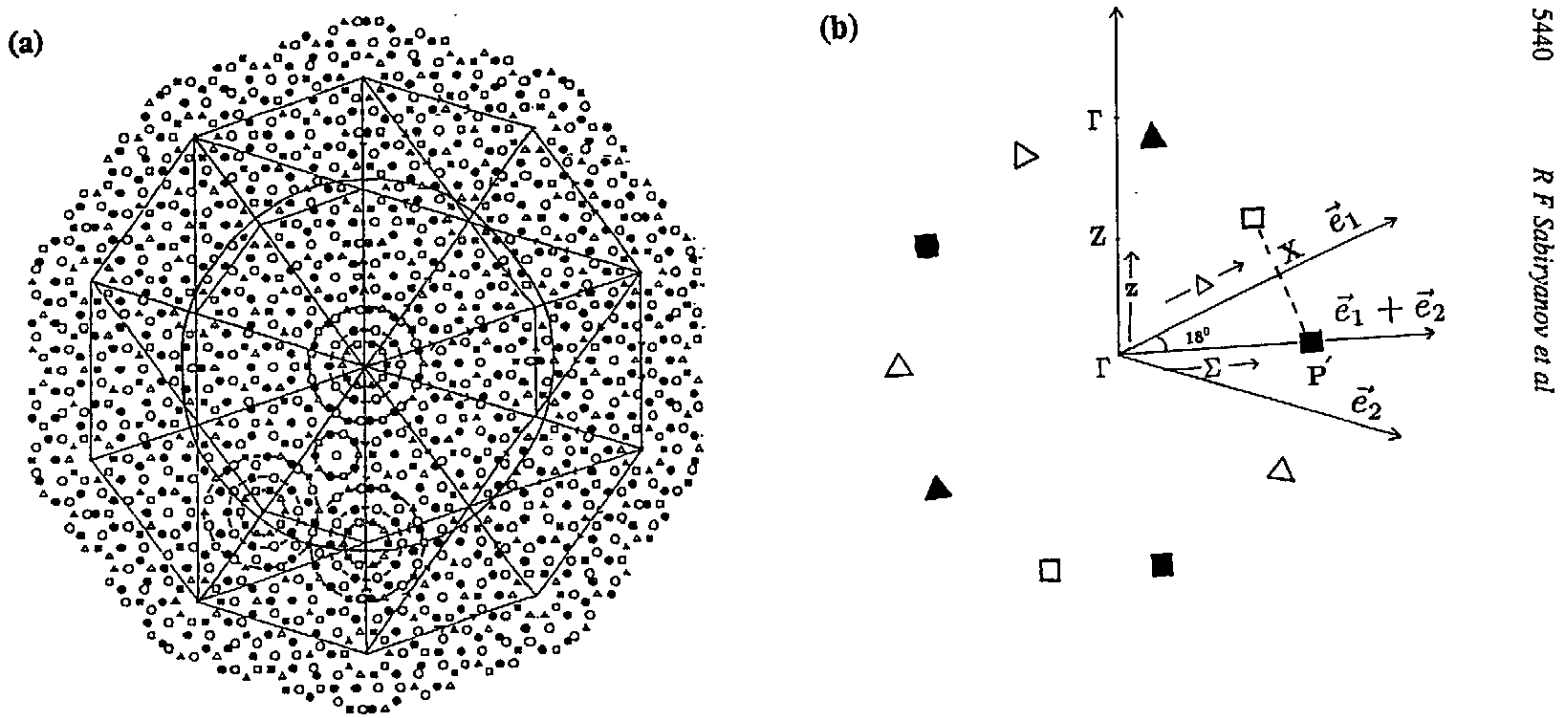

Figure 1. (*a*) Burkov model of the decagonal quasicrystal Al–Cu–Co: ○, Al; △, Cu; □, Co; empty symbols mark the $z = 0$ layer, full symbols the $z = c/2$ layer. Three large and one small atomic motifs (LAM and SAM) are shown explicitly; the LAM occupyies the vertices of the Klotz triangles [26]. The large circle centred at the origin of the cluster shows the boundary of the 198-atom (per plane) cluster used in the recursion calculation, which employs six repetitions of the 396-atom (counting the two layers shown) cluster in the z direction with a period 4.08 Å. The resulting 2376-atom cluster, with the atom types as shown here, is called the Burkov cluster. Clusters 1–5 are obtained from this basic cluster by interchanging positions and types of atoms as indicated in table 1 and at the end of section 2. (*b*) Symmetry directions in the quasiperiodic plane: Δ, Σ, and P′X, and along the periodic z axis (⊥ to the quasiperiodic plane): ΓZ, for which the spectral functions are studied. Γ is the origin of the cluster in the quasiperiodic xy plane. Σ is the direction joining the origin to one of the atoms in the atomic ring closest to the origin; P′ is the point on the Jones zone boundary in this direction. The symmetry direction Δ is at 18° to the direction Σ; X is the point on the corresponding Jones zone boundary. With the basis vectors (e_i, $i = 1, \ldots, 10$) directed along the sides of the Klotz triangles [26] at the origin of the cluster, the directions Δ and Σ are along the vectors e_i and $e_i + e_{i+1}$, respectively. Z is the centre of the Jones zone boundary in the z direction.

are certain experimental indications [27] that at low temperatures nature favours a different relative ratio of Cu to Co, namely $Cu_{\tau-3}Co_{\tau-4}$. The models referred to as clusters 2 and 4 (the last one was originally proposed in [14]), are very close in composition to this ideal ratio. We rate these two models as the favourite ones in reflecting the structure of true stable decagonal quasicrystals, though no judgment can be passed until more experimental data become available. Cluster 5 is the same as cluster 2, with the ring interchange in LAM as proposed by Phillips and Widom [13]. Cluster 3 was chosen to see the effect of drastically increasing the Cu concentration. Structures with a higher Co concentration than Cu have not been studied in this work, since most experimental works on decagonal Al–Cu–Co systems appear to have been done on samples with either equal Cu and Co concentrations or with a Cu concentration higher than Co.

Table 1. Band energies (1) and Fermi level DOS for the various clusters along with their specifications. Burkov: cluster with atom locations exactly as in figure 1 of this paper or figure 1(*a*) of [11a]; cluster 1: the cluster with the second and first rings in LAM of Burkov cluster interchanged according to the recommendation of Phillips and Widom [13]; cluster 2: the cluster with the Co atoms in the third shell of the LAM of Burkov cluster changed to Cu; cluster 3: the cluster with the third shell remaining the same as in the Burkov model, but all other locations of TM atoms occupied by Cu; cluster 4: the cluster with the third shell in the LAM of Burkov cluster being occupied by Co, and other TM locations being occupied by Cu; cluster 5: the same as cluster 2 with the ring interchange in LAM proposed by Phillips and Widom [13].

Cluster	Composition[a]	Band energy (Ryd/atom)	$N(E_F)$ (states/Ryd atom spin)	$N_d(E_F)/N(E_F)$
Burkov	$Al_{61}Cu_{19}Co_{19}$	−0.9183	2.22	0.57
Cluster 1	$Al_{61}Cu_{19}Co_{19}$	−1.6098	3.44	0.70
Cluster 2	$Al_{61}Cu_{26}Co_{13}$	−1.1916	1.56	0.50
Cluster 3	$Al_{61}Cu_{33}Co_{6}$	−0.9949	2.53	0.58
Cluster 4	$Al_{61}Cu_{27}Co_{12}$	−0.1604	2.22	0.60
Cluster 5	$Al_{61}Cu_{26}Co_{13}$	−1.7810	2.56	0.62

[a] The composition is given to the nearest correct two digits for the finite clusters used in the calculation.

3. Electronic structure and stability

Our results for decagonal Al–Cu–Co are based on recursion method [22] calculations performed in the tight-binding linear muffin-tin orbital (TB-LMTO) basis [21a] for clusters containing 2376 atoms. These clusters consist of 12 layers (parallel planes), with 198 atoms in each layer. In figure 1(*a*) the large circle at the centre of the Burkov model shows the boundary of the 198-atom (per plane) cluster used in the recursion calculation. Since figure 1(*a*) shows two planes of atoms, the total number of atoms within the circular boundary shown is 396. The 2376-atom cluster is obtained by repeating this 396-atom cluster six times in the z direction. The basic Burkov model cluster, which we refer to as the Burkov cluster in our discussions, is the one in which the positions of the Cu and the Co atoms are as described in the caption of figure 1(*a*). It has an equal number of Cu and Co atoms and is compositionally close to $Al_{\tau-1}Cu_{\tau'}Co_{\tau'}$, $\tau' = (2-\tau)/2$. The five other clusters studied by us (and referred to as cluster 1, cluster 2 etc) are just modifications of

this basic cluster, obtained by changing positions and types of atoms as described in the caption of table 1, and in the last paragraph of section 2.

We consider the Al, Cu and Co atoms in all inequivalent locations in the central region of a cluster and obtain the projected DOS on these atoms using the recursion method. The average DOS for the cluster is obtained from the proper weighted average of the atom-projected densities of states. The one-electron Hamiltonian is represented in the TB-LMTO basis using free boundary conditions in the z direction as well as in the xy plane, i.e. there are no matrix elements of the Hamiltonian connecting atoms across the faces of the cluster. Self-consistency in charge density and potential is achieved using the density functional theory with the local density approximation. Sphere radii are chosen such that the self-consistent electronic structure yields approximately charge neutral spheres. The exchange–correlation energy functional of von Barth and Hedin [28] is used. The local orbital-projected densities of states are obtained from the imaginary parts of the diagonal elements of the one-electron Green function expressed as a continued fraction. We have used different ways of terminating the continued fraction expansion of the Green function, namely the methods of Beer and Pettifor [29a] and Allan [29b]. We have also checked the stability of our results by varying the number of continued fraction coefficients. The results presented here were obtained by using the Beer–Pettifor terminator [29a] and typically 10s, 15p and 30d coefficients. The terminator due to Allan [29b] yielded similar results. Readers interested in the details of the TB-LMTO recursion method may consult [30].

The DOS for decagonal $Al_{\tau-1}Cu_{\tau'}Co_{\tau'}$, $\tau' = (2-\tau)/2$ (i.e. for the basic Burkov cluster) is shown in figure 2(a). For the sake of comparison, in figures 2(b) and 2(c) we present the DOS of the crystalline alloys $Al_{60}Cu_{20}Co_{20}$ and $Al_{60}Cu_{30}Co_{10}$, respectively. The DOS for these crystalline alloys are calculated via the standard (k-space) LMTO method using the atomic sphere approximation (ASA) [21b]. The same exchange–correlation potential (von Barth and Hedin [28]) is used in the k-space LMTO–ASA calculation (for figures 2(b) and (c)) as in the TB-LMTO recursion calculation (for figure 2(a)). In the ASA one replaces the muffin-tin spheres with space-filling, and therefore slightly overlapping, Wigner–Seitz spheres and neglects the remaining interstitial region. The method yields reliable results for all close-packed structures, as well as those open structures that can be close packed with the addition of interstitial ('empty') spheres. In our calculation the errors due to ASA are minimized by using the combined correction as described in [21b], where all the details of the LMTO–ASA method are also available.

The crystalline alloy $Al_{60}Cu_{30}Co_{10}$ exists in a thermodynamically stable trigonal (Al_3Ni_2 type, but 10 atoms per unit cell) structure [23] with $a = 4.112$ Å and $c = 9.916$ Å (space group $P\bar{3}m1$). The crystalline alloy $Al_{60}Cu_{20}Co_{20}$ is somewhat hypothetical in the sense that it is not thermodynamically stable, although there are indications [23] that disorder in the location of Cu and Co atoms may stabilize this alloy in the same structure (Al_3Ni_2 type, five atoms per unit cell, $a = 4.112$ Å and $c = 4.958$ Å) as $Al_{60}Cu_{30}Co_{10}$. The former is included in our study simply because it has equal numbers of Cu and Co atoms and is thus suitable for comparison with the Burkov cluster for decagonal Cu–Al–Co with equal Cu and Co concentrations. The DOS in figures 2(b) and (c) for crystalline $Al_{60}Cu_{20}Co_{20}$ and $Al_{60}Cu_{30}Co_{10}$, respectively, are obtained using five-atom and 10-atom unit cells with atom positions as specified in [23]. As can be seen in figure 2(c), there is a small minimum in the DOS at E_F for the thermodynamically stable crystal $Al_{60}Cu_{30}Co_{10}$, and our calculation yields a slightly higher cohesive energy for this crystal than for the hypothetical crystal $Al_{60}Cu_{20}Co_{20}$. Neither the Burkov cluster (figure 2(a)) nor crystalline $Al_{60}Cu_{20}Co_{20}$ (figure 2(b)) shows a local minimum in the DOS at the Fermi level. The implication is that for Cu to Co ratio equal to one, neither the decagonal phase nor its likely

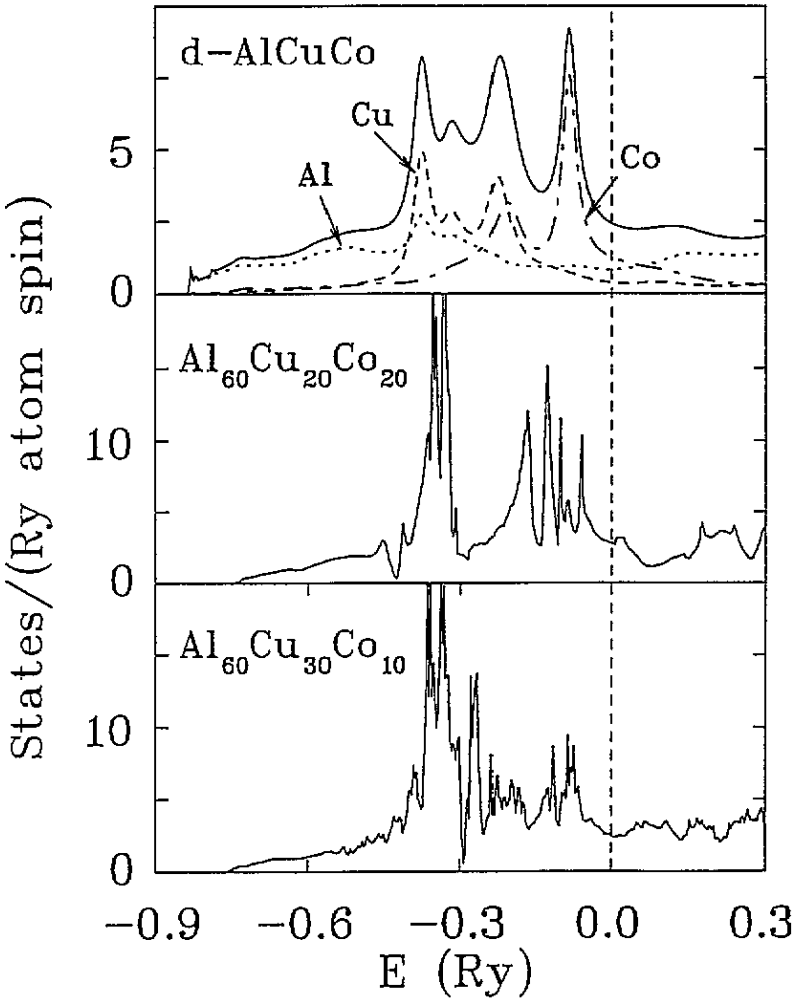

Figure 2. DOS for the Burkov cluster (figure 1) of decagonal Al–Cu–Co and its crystalline counterparts: (*a*) decagonal phase, (*b*) trigonal $Al_{60}Cu_{20}Co_{20}$ (may not be thermodynamically stable), (*c*) trigonal $Al_{60}Cu_{30}Co_{10}$ (thermodynamically stable). The zero of energy has been set to the Fermi level.

crystalline variant is stabilized via a Hume–Rothery mechanism, i.e. a pseudogap at the Fermi level.

Next, we consider variations on the Burkov model, as discussed in section 2. Our results are summarized in table 1 (the original model shown in figure 1 being labelled as Burkov, and the variations labelled as cluster 1, cluster 2, etc, as described in the caption to table 1). In figure 3 we show the DOS of these clusters, along with the contributions from the various component atoms. The zero of energy has been set at the Fermi level. Clusters 2 and 4 show minima in the DOS at E_F. Cluster 3 shows a shallower minimum, while clusters 1 and 5 do not. Looking at the component DOS we find that the local minima at E_F can arise due to different factors. For example, in cluster 3 the local minimum appears mainly from a small peak in the Co DOS slightly above the Fermi level, while in cluster 2 the minimum

is due to a sharp drop in the TM DOS around E_F, coupled with an increase in the Al DOS above E_F. Our analysis of DOS and spectral functions indicates that hybridization between TM d and Al s, p states is primarily responsible for the local minima in the DOS, rather than the FS–JZB interaction. Positions of the atoms in cluster 4 are similar to those in the crystalline approximant of the Burkov model presented by Trambly de Laissardiere and Fujiwara [14] using the standard LMTO–ASA method. The pseudogap in their crystalline (k-space) calculation is understandably somewhat deeper than that obtained by our real-space (recursion method) finite-cluster calculation. The magnitude of $N(E_F)$ for cluster 4 is about 50% higher than in the crystalline approximant calculation of [14]. It is clear from figure 3 that the shape and the magnitude of DOS at the Fermi level are strongly dependent on the locations and relative concentrations of Cu and Co atoms. This is in agreement with the conclusion reached by Trambly de Laissardiere and Fujiwara [14].

In table 1 we have presented the ratio of the d-orbital-projected DOS and the total DOS ($N_d(E_F)/N(E_F)$). This ratio shows that the eigenstates at the Fermi level for the various clusters used have roughly 40% s–p character. The mobility or the diffusivity (see [31,32] for a quantitative definition) of the s and p states in transition metal glasses or liquids is usually several times larger than that of the d states. For example, a TB-LMTO recursion study of liquid 3d transition metals [31] shows that the diffusivity of the s and p states in these systems is typically seven to 12 times larger than that of the d states. In decagonal quasicrystals, the diffusivity (hence the conductivity, which is the product of the DOS at the Fermi level and the diffusivity) in the direction of the tenfold axis is infinite due to periodicity. Finite conductivity in this direction can arise only due to phonons and defects. However, in the quasiperiodic plane finite diffusivity can result due to departure from periodicity and experience from transition metal glasses suggests that the in-plane diffusivity and conductivity should be dominated by the s and p states. Thus, while the stability and the binding energies of the decagonal Al–Cu–Co quasicrystals are dictated by the d states, and, therefore, the positions and concentrations of the TM atoms, their electrical conduction properties *in the quasiperiodic plane* should be dictated by s–p states and, therefore, the Al atoms.

In column 3 of table 1 we present the band energies per atom for the various clusters relative to the atomic energies defined as

$$E_b = \sum_{a,i} C_{a,i} \int^{E_F} \mathrm{d}E\, E\eta^{a,i}(E) - \sum_{a,l} C_a E_l^a N_l^a \tag{1}$$

where $\eta^{a,i}(E)$ is the DOS projected on to the atom of type a in one of its inequivalent locations i. E_F is the Fermi level. $C_{a,i}$ is the concentration of the atom type a in location i and $C_a = \sum_i C_{a,i}$. E_l^a is the energy level for the orbital quantum number, l, in a free atom of type a. N_l^a is the occupation of the energy level E_l^a in a free atom a. The integral in (1), which gives the one-electron band contribution to the total energy of the solid, includes the kinetic energy of the electrons, the Hartree (electron–electron Coulomb interaction) energy and the exchange–correlation energy. The latter two quantities are actually counted twice in this integral. Equation (1) would represent the cohesive energy if the first term on the right-hand side were replaced by the total energy. The total energy of the solid consists of this one-electron band term (the integral in (1)) plus an electrostatic term to account for the Coulomb repulsion of the ion cores, the correction for double counting the electron–electron Coulomb interaction and the exchange–correlation energy in the band term and a Madelung energy in case of charge transfer between atomic spheres. Since our atomic spheres are

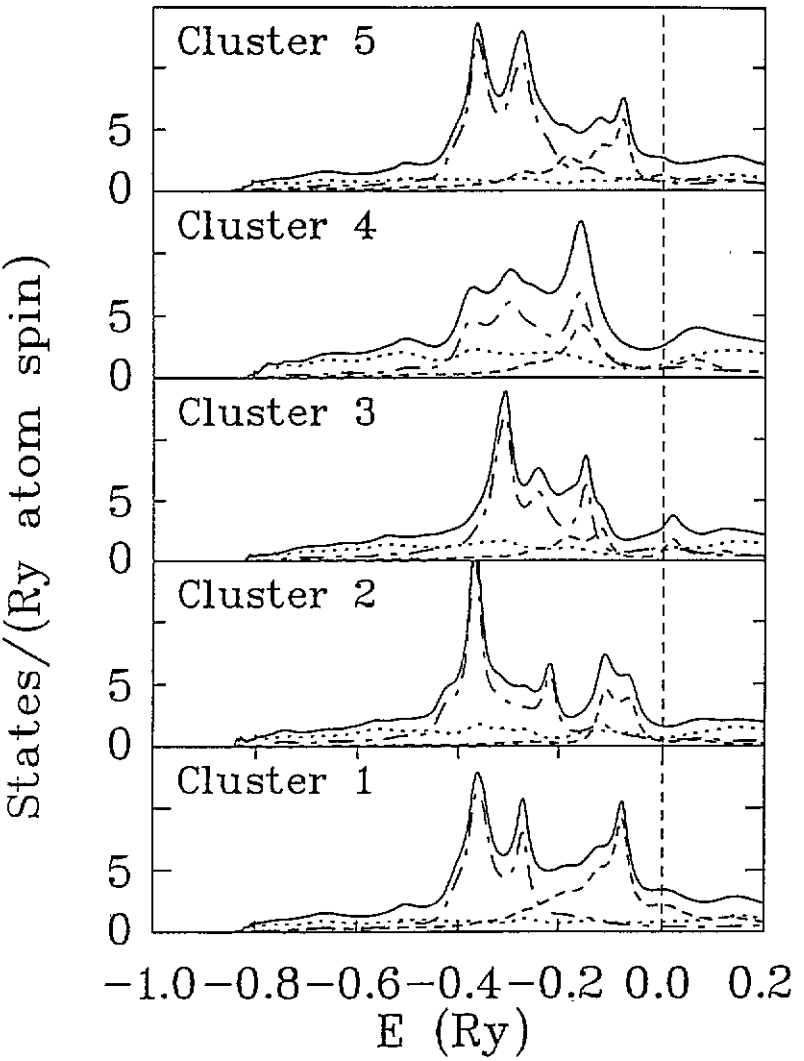

Figure 3. The DOS for various clusters. Full curve: total DOS; dotted curve: Al DOS; broken curve: Co DOS; long-dash and short-dash broken curves: Cu DOS. See table 1 for specification of the cluster labels. The zero of energy has been set to the Fermi level.

kept neutral this last term is zero in our calculations. In the absence of the electrostatic term E_b is not the cohesive energy. However, changes in this energy should reflect reasonably well the changes in total energies, as long as the lattice (in our case quasilattice) structure remains unaltered. For metallic alloys this prescription is known to approximate reasonably well the changes in the heat of formation [33, 34].

Among the clusters we have studied there is none with both a local minimum in the DOS at E_F and minimum internal energy. Note that for cluster 4, which shows the most pronounced local minimum in the DOS at E_F, the band energy is the highest. A local minimum in the DOS at the Fermi level only indicates that the given structure is favoured from the point of the band energy. It does not assure the local stability of the structure itself because a small change in the structure may strengthen the minimum. It implies local

stability *for the given structure* only against small changes in the composition and location of (some) atoms, assuming such changes do not alter the shape of the DOS, since such changes would move the Fermi level away from the minimum increasing the band energy (and therefore, most likely, the total energy as well). Thus if a system like cluster 4, with a DOS minimum at E_F but high band energy, is allowed the possibility of large changes in the concentrations and locations of Cu and Co atoms, it would certainly do so. From the view point of internal energy alone, the system will probably choose cluster 3, with a marginally different Cu/Co ratio, over cluster 4, since cluster 3 has a lower E_b, and also shows a local minimum (although a little less pronounced than for cluster 4) in the DOS at E_F (see figure 3 and table 1). We see that the Phillips and Widom prescription (cluster 1 of table 1) of moving the Al atoms from the second ring to the innermost ring in the LAM does lower the energy, as defined by (1).

A comment about the neglect of the electrostatic term is in order at this stage. As mentioned earlier, by keeping our spheres almost charge neutral we avoid the problem of having to calculate any Madelung term. We should examine how the neglect of the ion core repulsion affects our results. Since the Cu and Co cores have the same positive charge, interchanging the position of these atoms does not change the energy of repulsion of their ion cores and the change in the band energy is a very good measure of the change in total energy in this case. When the positions of Al and TM atoms are interchanged the electrostatic term due to ion core repulsion changes. However, in our study this happens only when we move the Al atoms from the second ring of LAM to the first (innermost) ring and correspondingly, the TM atoms from the first to the second. Since the Al core has less positive charge (three instead of 10) than Cu and Co, the electrostatic energy of repulsion when the Al atoms are in the first ring is less than when the first ring is occupied by the TM atoms. On top of this we find that even the band energy is reduced as a result of moving the Al atoms from the second to the first ring. Thus the inclusion of the electrostatic term would only reinforce our conclusion about the total energy being less for the Al atoms occupying the innermost ring of LAM.

To examine the differences in the internal energies of various clusters we have considered the atom-projected DOS. In figures 4–6, we show the DOS projected on to inequivalent Co and Cu atoms in three clusters. A comparison of the atom-projected DOS in figures 4 and 5 shows that moving Al atoms from the second to the innermost ring in the LAM, as suggested by Phillips and Widom [13], results in considerable lowering in the energies of the TM atoms. Similarly in cluster 4, which shows the most pronounced DOS minimum at E_F, the energy is higher mainly because the energy of Cu atoms has gone up. Note that the Cu_2 atoms in cluster 4 are the most abundant ones. The Al DOS, which is more or less spread over the entire energy range, does not change as strongly as the TM DOS from one cluster to another. The contribution of the Al atoms to the total binding energy is small compared with that of the TM atoms. In figure 7 we show the DOS of the two most abundant Al atoms in the Burkov model and in cluster 4. The Al DOS for cluster 4 shows a more pronounced minimum at E_F. Looking at the partial (orbital-projected) DOS we find that this minimum is mainly due to a minimum in the p DOS. Our study of the spectral functions (see section 4) reveals that this minimum is due to the p–d hybridization, and not due to scattering of the p electrons of energy E_F by the quasiperiodic potential at the Jones zone boundary.

Extensive experimental work by Grushko [27] shows that the decagonal phase in the Al–Cu–Co system is stable in the temperature range 550–1000 °C. The low-temperature phases contain more Cu than Co. Clusters 2–5 studied by us are thus among the likely low-temperature structures. Among these, cluster 4, with the deepest pseudogap, has the

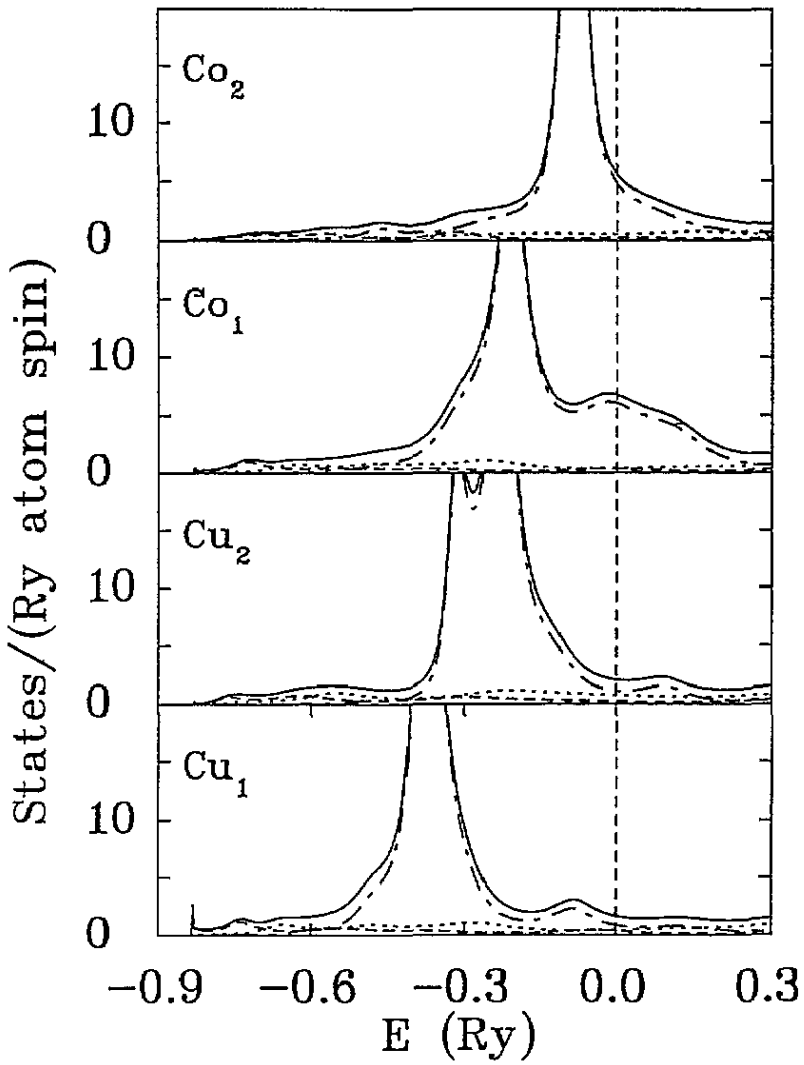

Figure 4. TM-atom-projected DOS in the Burkov cluster. Subscript 1 refers to TM atoms in the third shell of the LAM. Subscript 2 refers to the average of the SAM DOS and that of the innermost ring of the LAM. The zero of energy has been set to the Fermi level (full curve, total DOS; broken curve, s DOS; dotted curve, p DOS; long- and short-dash broken curve, d DOS).

maximum local stability. Clusters 2 and 3 have lower internal energies, but shallower minima in the DOS at E_F. Clusters 1 and 5, obtained by the Phillips and Widom ring interchange [13], are inconsistent with the diffraction results and have no local minima in the DOS at E_F, i.e. no local stability against small changes in composition and locations of atoms. The fact that these two clusters have lower energy than all the other clusters indicates that the Burkov model, although consistent with the diffraction results, does not allocate atomic positions corresponding to minimum internal energy.

With increasing temperature there can be larger variations in the relative concentrations of the TM atoms. Phases with roughly equal amounts of Cu and Co become stable at higher temperatures [27]. The clusters with equal Cu–Co composition (Burkov cluster,

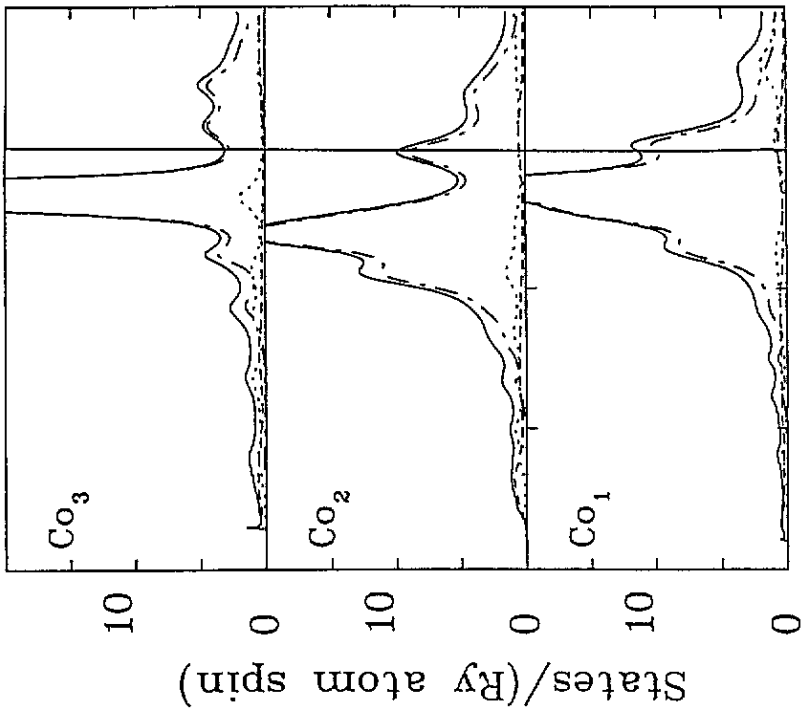

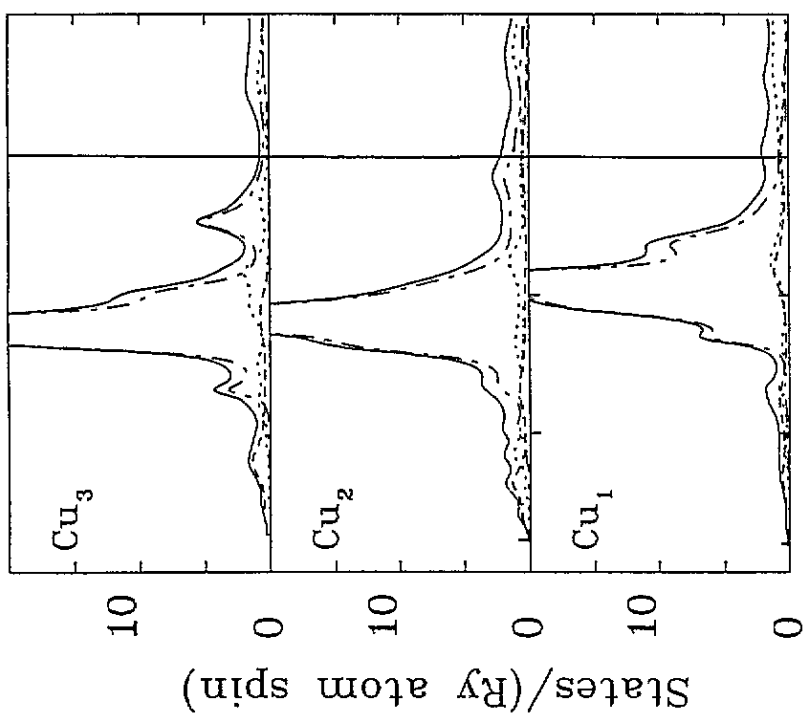

Figure 5. TM-atom-projected DOS in cluster 1, incorporating the Phillips and Widom LAM ring interchange; (*a*) Cu DOS, Cu_1: Cu in the second shell of the LAM; Cu_2: Cu in the third shell of the LAM; Cu_3: Cu in the SAM; (*b*) Co DOS with the subscript having the same connotation as in (*a*). The zero of energy has been set to the Fermi level (the meaning of the various curves is the same as in figure 4).

cluster 1) are neither the lowest-energy clusters according to our calculation, nor do they show any local minimum in the DOS at E_F. It is possible that such compositions become thermodynamically stable due to a minimum in the free energy rather than in the internal energy. If we consider the changes in free energy as a result of changes in the Cu/Co ratio (with the possibility of complete disorder in the locations of these atoms, with the Al positions fixed), then at a given temperature the free energy is a minimum (the entropy is a maximum) for Cu/Co = 1. We have calculated the energy change associated with interchanging Cu and Co atoms. Within a given ring the energy change is very small, varying between −0.11 mRyd and 0.21 mRyd per such Cu–Co interchange. But these interchanges can give rise to an entropy change, such that the free energy change becomes the dominant factor in stabilization. This may also be the reason why the crystalline structure $Al_{60}Cu_{20}Co_{20}$ is not thermodynamically stable, while the quasicrystalline phase $Al_{62}Cu_{19}Co_{19}$, with the possibility of disorder in the positions of Cu and Co atoms within a given ring, is stable. A similar conclusion regarding the stability of icosahedral AlZnMg against the corresponding crystalline approximants was arrived at by Hafner and Krajči [15]. In order to verify this possibility one needs to calculate accurately the free energies for various clusters. This is a difficult task even for crystalline systems.

4. Spectral functions

Whether or not an electron–lattice interaction at wave vectors corresponding to a (pseudo) Jones zone boundary is responsible for certain features of the DOS can be explored via spectral functions [30, 31], $S(k, E)$. For certain icosahedral quasicrystals this has been done by Hafner and Krajči [15, 16]. Niizeki and Akamatsu [35] have studied the spectral densities in a 2D Penrose lattice, but no theoretical study of spectral functions for *real* decagonal quasicrystals has as yet been presented. We calculate $S(k, E)$ as the DOS projected onto a Bloch-like combination of the orbitals in the cluster, as described in [31]. By following the peaks in $S(k, E)$ for various wave vectors, k, one can map an effective dispersion relation (E against k) for the energy eigenstates. The absence of any pronounced peak in $S(k, E)$ indicates the inappropriateness of the corresponding k values in describing the eigenstates of the system.

The high-symmetry points and the high-symmetry axes for decagonal quasicrystals have been completely enumerated by Niizeki [36]. There are 10 classes of high-symmetry axes in the quasiperiodic plane for a decagonal quasicrystal. We calculate the spectral functions along three of the symmetry axes in the quasiperiodic plane and the z axis, the direction of periodicity. In figure 1(b) we have shown these symmetry directions. The notation we use follows closely that of Niizeki [36]. Γ represents the origin of the cluster in the xy plane. One can introduce 10 basis vectors (e_i, $i = 1, \ldots, 10$) directed along the sides of the Klotz triangles [26] at the origin of the cluster. Then Σ is the direction joining the origin to one of the atoms in the atomic ring closest to the origin (say, along the vector $e_1 + e_2$), with the point P′ being on the Jones zone boundary (i.e. ΓP′ is half the strongest scattering vector in the direction Σ). The symmetry direction Δ, along the vector e_1, makes an angle of 18° with this direction and X is the point on the JZB in this direction. The notation Z is used to denote the centre of the Jones zone boundary in the z direction.

In figure 8(a) we show $S(k, E)$ along the symmetry direction Σ in the quasiperiodic reciprocal (k_x, k_y) plane, calculated for the basic Burkov cluster (large circle centred about the origin in figure 1(a)). Figure 9(a) shows the same for the periodic ΓZ direction. In the (b) parts of the corresponding figures we show the E against k relations as deduced from

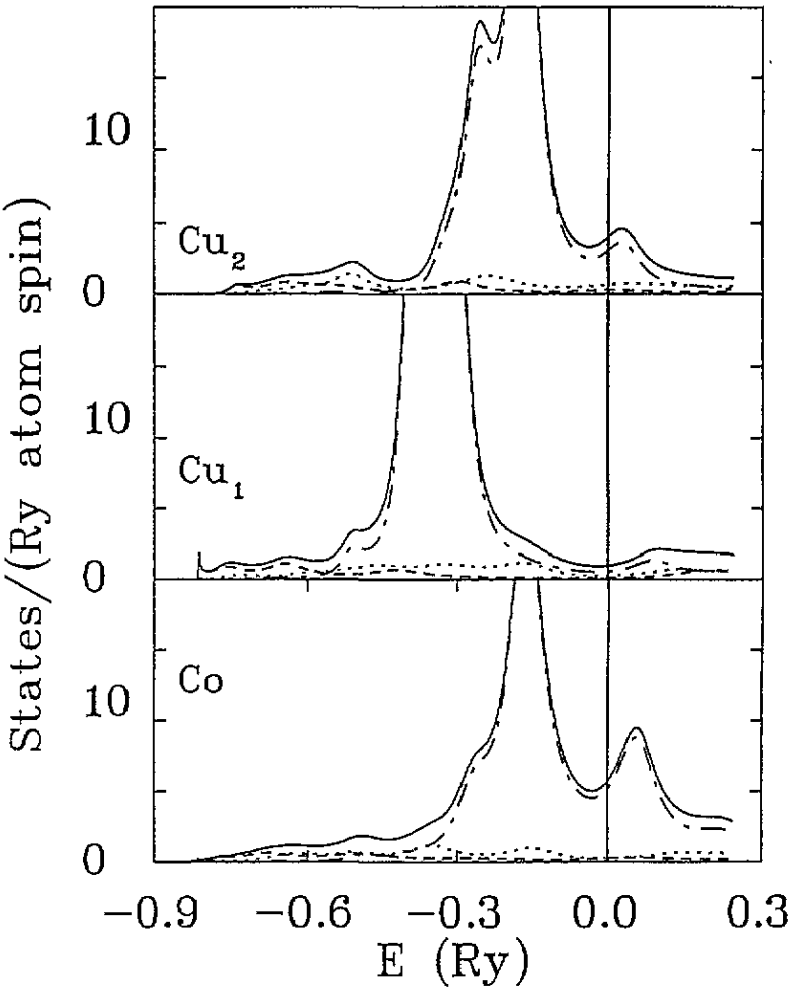

Figure 6. TM-atom-projected DOS in cluster 4. Co in the third shell of the LAM. Cu_1: Cu in the SAM; Cu_2: Cu in the innermost ring of the LAM. The zero of energy has been set to the Fermi level (the meaning of the various curves is the same as in figure 4).

the peaks in $S(k, E)$. Figure 10 is a schematic quasi-band structure for the Burkov cluster, deduced from the peaks in $S(k, E)$. Figure 11 is a similarly deduced quasi-band structure for cluster 4, where the spectral function is shown resolved into various orbital components denoted by different symbols. In figures 8(*b*), 9(*b*), 10 and 11, the points obtained from the positions of the peaks in the spectral function have been joined by hand simply to guide the eye. No symmetry analysis was done to determine crossing or noncrossing of bands.

The first three sections of figure 10 (Γ–X, X–P′, P′–Γ) show the bands in the quasiperiodic plane and the last section shows the bands in the z direction. It is interesting to see that our real-space calculations, based on finite-size clusters with free boundaries, reveal clearly the periodic distribution of the Γ points (in the extended zone scheme) along k_z, and their quasiperiodic distribution in the (k_x, k_y) plane. This is in sharp contrast with the behaviour of $S(k, E)$ in amorphous materials [30], where sharp peaks appear only for small value of k corresponding to wavelengths many times the nearest-neighbour separation.

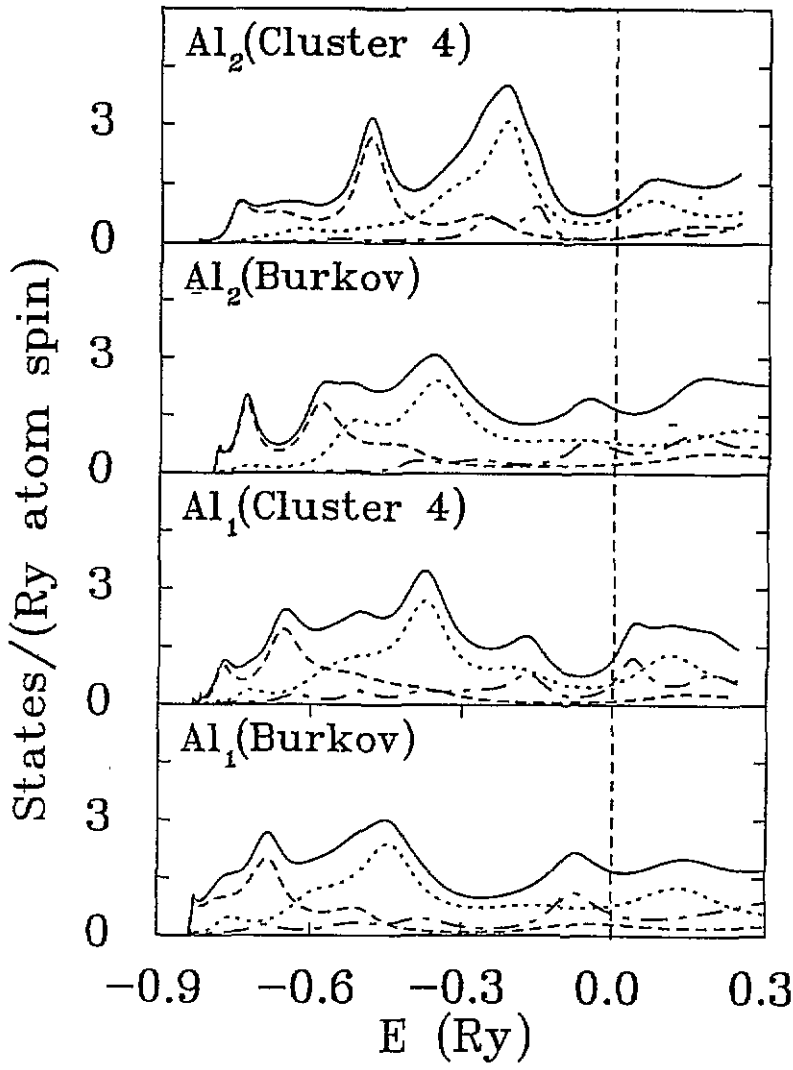

Figure 7. Atom-projected DOS for the two most abundant Al atoms in the Burkov cluster and cluster 4. The zero of energy has been set to the Fermi level (the meaning of the various curves is the same as in figure 4).

Note also that the periodicity in the z direction emerging from our calculations is twice the periodicity one expects from simple geometrical considerations. The expected value of the period in the z direction is $2\pi/c$ where $c = 4.08$ Å. This yields a value of $1.54\,\text{Å}^{-1}$, whereas our calculations reveal that, in figures 9 and 10, $\Gamma Z = 1.54\,\text{Å}^{-1}$, i.e. periodicity in the z direction of $3.08\,\text{Å}^{-1}$. This effect was predicted by Lück and Kek [37] solely on symmetry considerations: the decagonal quasicrystal possesses a screw axis, very much like the h.c.p. structure, resulting effectively in obliteration of the odd Bragg planes at $(2n+1)\pi/c$, again reminiscent of what happens in the h.c.p. structure. The peak positions in $S(\boldsymbol{k}, E)$ in the (k_x, k_y) plane are related to the positions of atoms in the Klotz triangle tiling [26] used in the Burkov model [11a]. This tiling gives rise to more than one (quasi)periodicity,

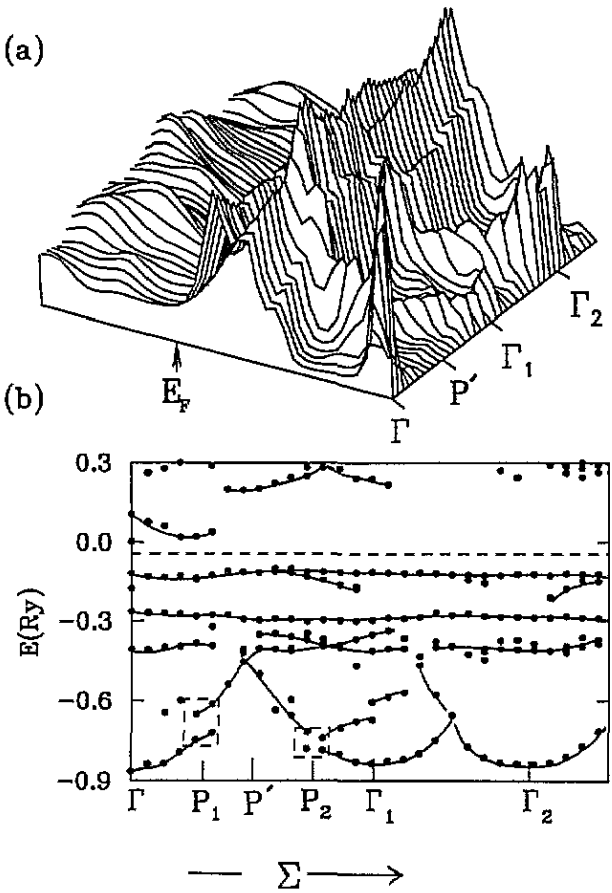

Figure 8. Spectral function (*a*) and quasi-band structure (*b*) along the symmetry direction Σ (see figure 1(*b*) for reference) in the quasiperiodic (k_x, k_y) plane in decagonal Al–Cu–Co for the Burkov cluster. The horizontal broken line shows the Fermi level. In (*b*) the points obtained from the positions of the peaks in the spectral function have been joined by hand simply to guide the eye. No symmetry analysis was done to determine crossing or noncrossing of bands.

involving different groups of atoms and dictated by τ, along the symmetry directions in the (x, y) plane. This is reflected in $S(k, E)$ shown in figure 8. In figure 8(*b*) the smallest period is $3.08\,\text{Å}^{-1}$ (Γ_1), and JZB along this symmetry line is at $\text{P}' = 1.54\,\text{Å}^{-1}$. The next Γ point ($\Gamma_2$) is at $5.05\,\text{Å}^{-1}$, with $\Gamma\Gamma_2/\Gamma\Gamma_1 = \tau$. Additional features appear in $S(k, E)$ at effective or quasi-Brillouin zone boundaries (qBZB). We have identified with boxes two such noticeable features in figure 8(*b*), one outside (at P_2) and the other inside (at P_1) the JZB, P. We find that $\Gamma\text{P}_2/\Gamma\text{P}' = \Gamma\text{P}'/\Gamma\text{P}_1 = \tau$. The quasi-band structure consists of parabolic s bands in the low-energy region. Closer to (but below) E_F the bands are mostly d-like and dispersionless, indicating a high effective mass for the carriers in these states. Near and at E_F there are both flat (dispersionless) and parabolic bands, although this may not be clear from the plot of the most intense peaks shown in figure 10. A vestige of gaps as a result of parabolic s band and qBZB interaction appears at energies much below E_F (see boxed features in figure 8(*b*) and 10), but such gaps do not extend across the entire zone. No such feature, originating from FS–JZB (or qBZB) interaction, can be detected in

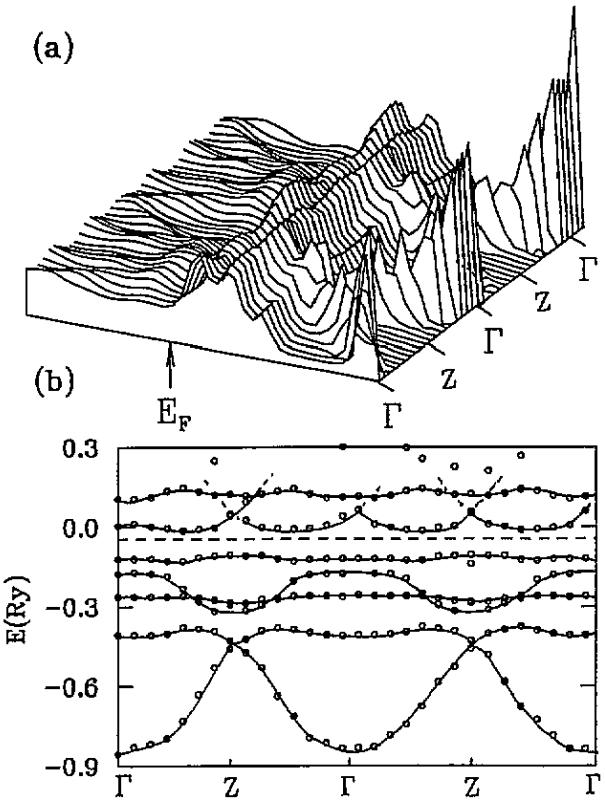

Figure 9. Same as figure 8, along the periodic k_z direction. Z denotes the point on the Jones zone boundary in this direction.

the bands near E_F. There are also features indicative of the interaction at qBZB, which do not seem to result in noticeable gaps (such as the one marked with ? in figure 10). Note that while a gap like the one marked by a square in figure 10 can be believed to be due to a free-electron getting scattered by a quasiperiodic lattice at one of the possible quasi-Brillouin zone boundaries, a gap like X_1X_2 in the s band appearing at the Jones zone boundary X in figure 10 is due to the s–d hybridization. Without the hybridization this gap would have been much narrower and far below the Fermi level.

In figure 11 we show the (quasi)band structure for cluster 4, which shows the most pronounced DOS minimum at E_F. If the FS–JZB interaction is at all responsible for this pseudogap, we should see some indication of that in the spectral functions, as observed by Hafner and Krajči [15, 16] for icosahedral quasicrystals. The situation as depicted by figure 11 is different from that in icosahedral quasicrystals. Spectral functions for icosahedral quasicrystals studied by Hafner and Krajči [15, 16] show a series of highly degenerate free electron states near the Fermi level. Such states do not appear in our calculation. There are virtually no s bands appearing near the Fermi level, in the quasiperiodic (k_x, k_y) plane.

The band structure presented in figure 11 reveals the presence of an s band (parabolic) near the Fermi level in the k_z direction. Presumably such parabolic s bands are also present in the k_z direction for other clusters. In figures 9 and 10 (for the original Burkov cluster) the shape of this band is somewhat different, due to different hybridization effects. In the quasiperiodic plane mostly flat bands seem to appear near E_F. Parabolic free-electron-like

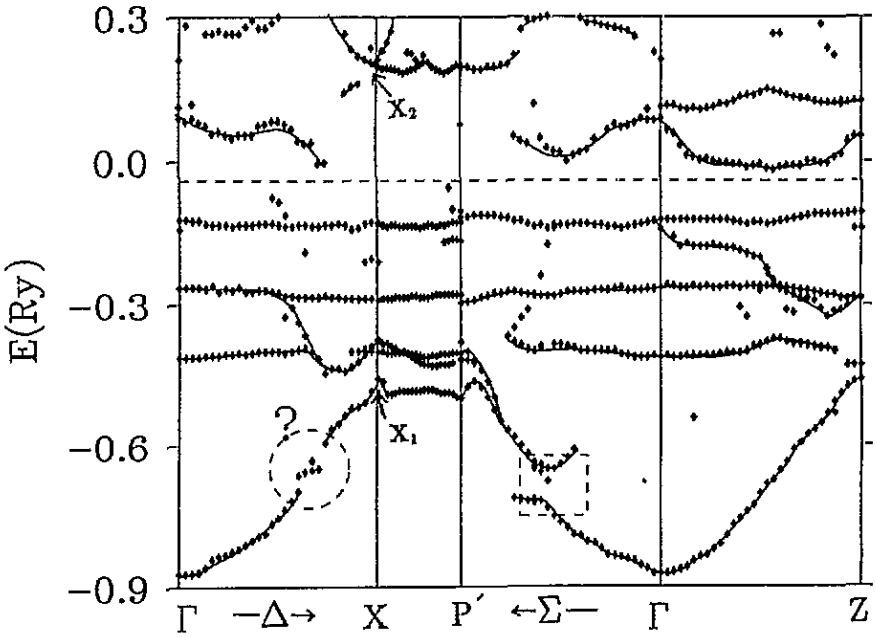

Figure 10. Quasi-band structure in the Burkov cluster for decagonal Al–Cu–Co as deduced from spectral functions. The symmetry directions are indicated in figure 1(*b*). The horizontal broken line shows the Fermi level. The points obtained from the positions of the peaks in the spectral function have been joined by hand simply to guide the eye. No symmetry analysis was done to determine crossing or noncrossing of bands.

bands near E_F in the z direction and less dispersive flat bands in the quasiperiodic plane may be responsible for the large anisotropy in the in-plane and out-of-plane conduction, as observed by Basov and co-workers [10]. Although this may not be absolutely clear from the spectral function based on our real-space calculations, this view is strongly supported by a decagonal plane-wave model calculation recently reported by us [38].

To summarize this section, our spectral function calculation based on clusters with free boundaries reveals the periodicity and the quasiperiodicity of the model, but does not provide any evidence of a FS–JZB. As mentioned in the beginning of this section, there are 10 classes of high-symmetry axes in the quasiperiodic xy plane, and we have studied the spectral function along only three of these, in addition to the z direction. The primary purpose here was to see whether there is any indication of energy gaps opening up at JZB due to interaction of nearly free electrons with the (quasi)lattice. There is no strong evidence of this from the spectral functions for the four symmetry directions considered.

5. Localization in the Burkov model

The results of the previous section show that k is most likely a good quantum number for the three symmetry directions in the quasiperiodic plane for which spectral functions were studied. In the absence of the Bloch theorem, however, one cannot rule out the possibility that the eigenstates in the quasiperiodic plane, in some energy regions, are localized or critically localized. Note that the eigenstates are extended in the z direction as a result of periodicity.

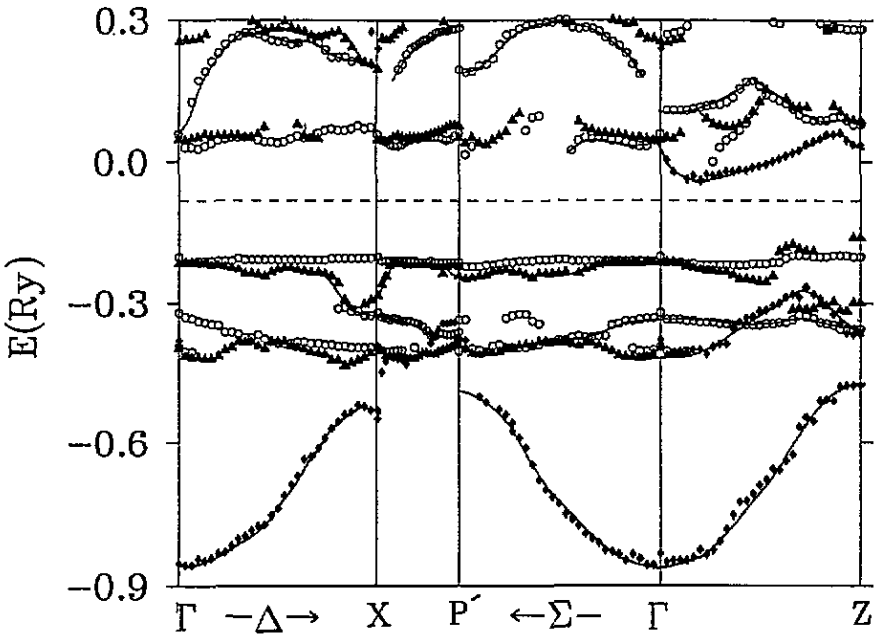

Figure 11. Quasi-band structure in cluster 4 for decagonal Al–Cu–Co, as deduced from spectral functions. The symmetry directions are indicated in figure 1(*b*). The horizontal broken line shows the Fermi level. s, p and d bands are shown separately with full rectangles, triangles and empty circles, respectively. The points obtained from the positions of the peaks in the spectral function have been joined by hand simply to guide the eye. No symmetry analysis was done to determine crossing or noncrossing of bands.

Measurement of the optical conductivity of high-quality decagonal quasicrystals $Al_{65}Co_{17}Cu_{18}$ and $Al_{62}Co_{15}Cu_{20}Si_3$ by Basov and co-workers [10] shows a strong anisotropy between the periodic and quasiperiodic directions. The FIR resistivity in the periodic direction is about 10 times smaller than that in the quasiperiodic plane. The latter is about two to 2.5 times larger than that of strong-scattering metallic glasses and liquid metals. While the resistivity in the periodic z direction is due to phonons and defects, the increased resistivity in the planes could be caused by a drastic increase in the scattering rate due to quasiperiodic order. Alternatively, the increased in-plane resistivity could be due to some sort of weak localization or critical nature [25] (neither extended nor localized) of the states in the plane. Diffusivity (as in [31]) of the critical states, and hence their contribution to the conductivity, should be substantially lower than that of the extended states. To study the localization of the eigenstates at the Fermi level we have used the concept of the generalized participation ratio [24] or the p-(pseudo)norm

$$\alpha_p = \sum_i |a_i|^{2p} \left(\sum_i |a_i|^2 \right)^{-p} \tag{2}$$

discussed by Tsunetsugu and co-workers [25] in the study of localization in two-dimensional Penrose tiling. Here the a_i are the weights of the eigenstates on the orbitals in the cluster. The eigenstates at E_F were calculated using the filtering technique discussed in [39]. In figure 12 we show the variation of α with the number of atoms in the Burkov cluster (figure 1) for the $p = 2$ case only. The variations for the $p = 3$ and $p = 4$ cases are

qualitatively similar. Two sets of calculations were performed. In one case we considered two layers of atoms and gradually increased the number of atoms in the two layers (curve a). Next we kept the number of atoms in the quasiperiodic plane fixed at 198, and gradually added more and more layers (curve b). In view of the fact that the states are extended in the z direction the latter may appear a trivial exercise, but was performed to see whether the periodicity in the z direction has a negative effect on the localization in the quasiperiodic plane. For a completely extended state with equal weight on each orbital in the cluster, α_p should vary as N^{1-p}, where N is the number of atoms in the cluster. For localized states α_p should saturate at a value, indicative of the number of atoms over which the state is localized. There is no such saturation for the two cases within the clusters used in the calculation. Thus our calculation reveals no indication of localization within the span (50 Å) of the clusters used. The fact that the observed decrease in α_p is slower than N^{1-p} (curve c) is due to the fact that the weights on various orbitals are not the same, even though the state is extended. There is also a possibility of weak localization, with the localization length being larger than the maximum span of the clusters (50 Å) used. The decrease in α_p, when the number of atoms in the quasiperiodic layers is increased, is slower than when the number of layers is increased with the number of in-plane atoms held constant. This, since the eigenstates possess infinite localization length in the z direction due to periodicity, could be taken as an indication that the states are weakly localized in the xy plane with large but finite localization length. However, this is speculation: all that can be said with certainty is that the states are not localized within a span of 50 Å. We have carried out similar studies on a few other clusters from table 1, and the results remain qualitatively unchanged.

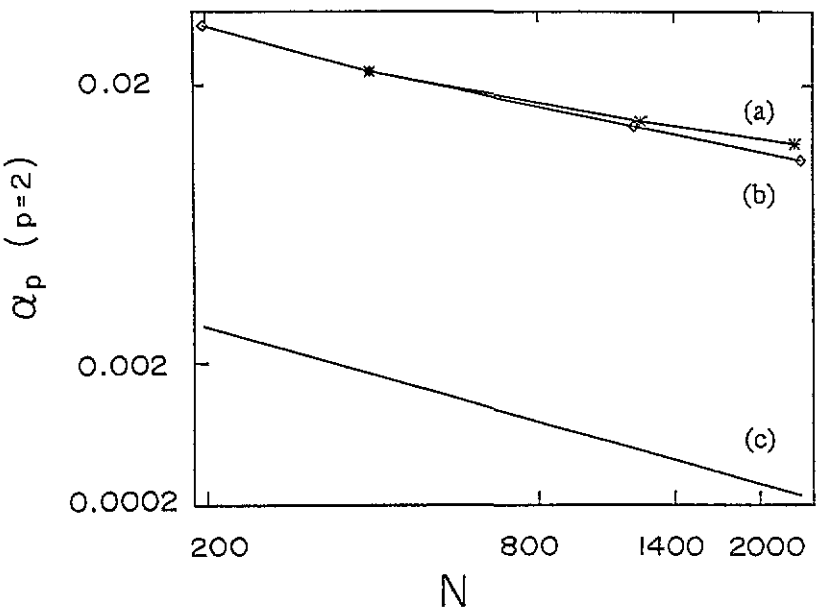

Figure 12. Variation of the pseudo-(p-)norm, α_p, of the wavefunction at the Fermi level with cluster size, N, on a log–log plot, for the Burkov cluster for decagonal Al–Cu–Co. See text for the distinction between the curves.

6. Conclusions

All our conclusions apply strictly to the Burkov model, and generalizations to decagonal quasicrystals at large should be made with reservation. The stability of the model depends crucially on the locations and concentrations of the two TM atoms. This is summarized in figure 13 (also table 1), where we indicate the shape of the DOS along with the band energies for the Burkov cluster and its variations. Some modifications show local minima in the DOS at E_F, indicating local stability against small changes in composition and location of TM atoms in the given structure. Cluster 4, with the most pronounced minimum, reflects the favourite structure from the viewpoint of such local stability. Clusters 2 and 3 have lower internal energies, but shallower minima in the DOS at E_F. All clusters with a local DOS minimum at or near E_F have substantially higher Cu (twice or more) concentration than Co.

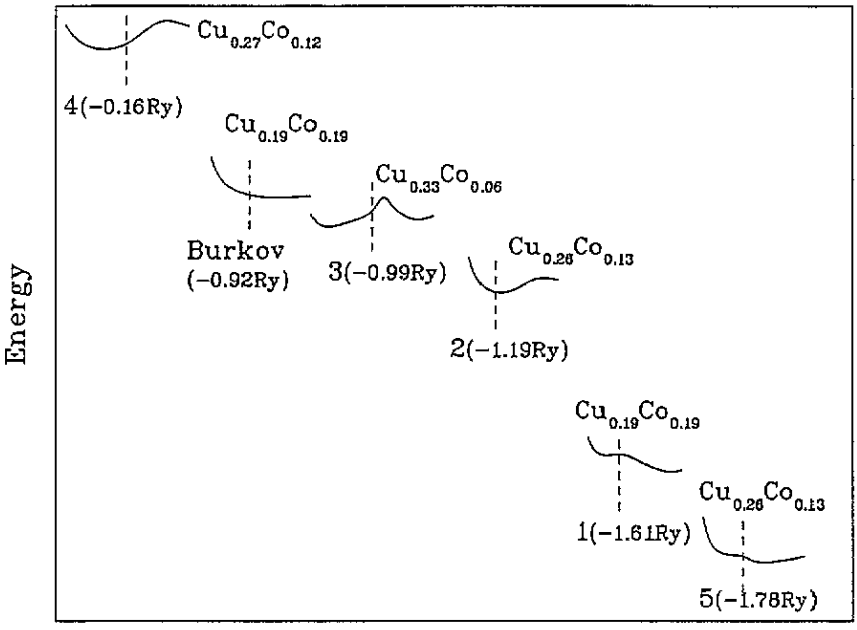

Figure 13. Band energies and the DOS near E_F for the Burkov cluster and its variations. The vertical line shows the position of the Fermi level. Cu and Co concentrations for the various clusters are also indicated.

The local minima in the DOS at E_F for clusters 2–4 are due to different shapes of the component atom DOS. The principal cause of these minima is the hybridization between Al s, p and TM d states, and not FS–JZB. This last conclusion is based on a study of spectral functions, which do not reveal any gaplike feature in the s bands near the Fermi level. Some gaplike features appear in s bands at wavevectors corresponding to some quasi-Brillouin zone boundaries, at energies much below E_F. Such gaps do not extend across the entire zone.

The original Burkov model as well as the model suggested by Phillips and Widom [13] (cluster 1) does not have a DOS minimum at E_F. Both of these models have equal

concentrations of Cu and Co atoms. We suggest that such structures might be stable due to a maximum in the entropy (minimum in free energy) associated with possible disorder in the locations of TM atoms [40]. This may also explain why experiments indicate that decagonal Al–Cu–Co quasicrystals with equal concentrations of Cu and Co are thermodynamically stable, while a crystalline structure with similar concentrations is not. Optical conductivity (including the IR and FIR region) measurements by Basov and co-workers [10], and more recently valence band photoemission experiments by Stadnik and co-workers [20], done on decagonal Al–Cu–Co samples with equal or nearly equal Cu and Co concentrations, report negatively on the existence of a pseudogap at E_F. These experiments as well as the results of the present paper strongly suggest that these alloys are not stabilized via the Hume–Rothery mechanism.

A decagonal plane-wave model calculation recently presented by us [38] reveals that the periodicity in the z direction is responsible for reducing or obliterating the pseudogap in the DOS. Nearly dispersionless bands in the quasiperiodic plane appear in this model, and show a gap in the DOS for a 2D system. For a 3D system, periodic in the z direction and quasiperiodic in the (x, y) plane, there are parabolic bands in the k_z direction running through the gap region. These parabolic bands destroy the gap and change it to only a shallow minimum in the DOS. This conclusion applies strictly to a free-electron-like system. The presence of TM atoms in real decagonal quasicrystals such as Al–Cu–Co will change this picture somewhat. Depending on the Al–TM band hybridization, there may sometimes be a weak pseudogap, and sometimes the pseudogap may be nonexistent, as observed in the present calculation.

Acknowledgments

Financial support for this work was provided by the Natural Sciences and Engineering Research Council of Canada. The authors are thankful to T Timusk and D Basov for helpful discussions. SEB would like to acknowledge useful discussions also with S J Poon and N Ashcroft. The work of SEB was supported by NSF grant DMR-9120199.

References

[1] Poon S J 1992 *Adv. Phys.* **41** 303
[2] Kortan A R, Thiel F A, Chen H S, Tsai A P, Inoue A and Masumoto T 1989 *Phys. Rev.* B **40** 9397
[3] Kortan A R, Becker R S, Thiel F A and Chen H S 1990 *Phys. Rev. Lett.* **64** 200
[4] Chen H, Burkov S E, He Y, Poon S J and Shiflet G J 1990 *Phys. Rev. Lett.* **65** 72
[5] Hiraga K, Sun W and Lincoln F J 1991 *Japan. J. Appl. Phys.* **30** L302; 1991 *Mater. Trans. JIM* **32** 308
[6] Launois P, Audier M, Dénoyer F, Dong C, Dubois J M and Lambert M 1990 *Europhys. Lett.* **13** 629
[7] Steurer W and Kuo K H 1990 *Phil. Mag. Lett.* **62** 175; 1990 *Acta Crystallogr.* B **46** 703
Kek S and Mayer J 1993 *Z. Kristallogr.* **205** 235
Steurer W, Haibach T, Zhang B, Kek S and Lück R 1993 *Acta Crystallogr.* B **49** 661
[8] Yamamoto A, Kato K, Shibuya T and Takeuchi S 1990 *Phys. Rev. Lett.* **65** 1603
[9] Dian-Lin Z, Shao-Chun C, Yun-Ping W, Li L, Xue-Mei W, Ma X L and Kuo K H 1991 *Phys. Rev. Lett.* **66** 2778
[10] Basov D N, Timusk T, Barakat F, Greedan J and Grushko B 1994 *Phys. Rev. Lett.* **72** 1937
[11a] Burkov S E 1993 *Phys. Rev.* B **47** 12325
[11b] Burkov S E 1991 *Phys. Rev. Lett.* **67** 614; 1992 *J. Physique* I **2** 695
Jena P, Khanna S N and Rao B K (ed) 1992 *Physics and Chemistry of Finite Systems: From Clusters to Crystals (NATO ASI series 374)* (Dordrecht: Kluwer) pp 77–83
[12] Henley C L 1993 *J. Non-Cryst. Solids* **153–4** 172

[13] Phillips R and Widom M 1993 *J. Non-Cryst. Solids* **153–4** 416
[14] Trambly de Laissardiere G and Fujiwara T 1994 *Mater. Sci. Eng.* A **179–80** 722; 1994 *Phys. Rev.* B **50** 9843
[15] Hafner J and Krajči M 1992 *Phys. Rev. Lett.* **68** 2321; 1992 *J. Non-Cryst. Sol.* **150** 337
[16] Hafner J and Krajči M 1993 *Phys. Rev.* B **47** 11 795
[17] Fujiwara T and Yokokawa T 1992 *Phys. Rev. Lett.* **66** 333
Fujiwara T 1989 *Phys. Rev.* B **40** 942
[18] Carlsson A E 1993 *Phys. Rev.* B **47** 2515; 1993 *J. Non-Cryst. Solids* **153–4** 386
Smith A P and Ashcroft N W 1987 *Phys. Rev. Lett.* **59** 1365
Friedel J 1988 *Helv. Phys. Acta* **61** 538
[19] Nagel S R and Tauc J 1975 *Phys. Rev. Lett.* **35** 380
[20a] Stadnik Z M, Zhang G W, Tsai A-P and Inoue A 1995 *Phys. Lett.* **198A** 237
[20b] Stadnik Z M and Stroink G 1993 *Phys. Rev.* B **47** 100; 1993 *J. Non-Cryst. Solids* **156–7** 891
[21a] Andersen O K 1975 *Phys. Rev.* B **12** 3060
Andersen O K, Jepsen O and Glötzel D 1985 *Highlights of Condensed Matter Theory* ed F Bassani, F Fumi and M P Tosi (Amsterdam: North-Holland) pp 59–176
Andersen O K, Jepsen O and Sob M 1987 *Electronic Structure and Its Applications (Lectures Notes in Physics 283)* ed M Yusouff (Berlin: Springer) pp 1–57
[21b] Andersen O K 1975 *Phys. Rev.* B **12** 3060
Skriver H L 1984 *The LMTO Method (Springer Series in Solid State Sciences 41)* ed M Cardona, P Fulde and H-J Queisser (Berlin: Springer)
[22] Haydock R 1980 *Solid State Physics 35* ed F Seitz and D Turnbull (New York: Academic) p 215
[23] Grushko B, Urban K and Freiburg Ch 1991 *Scr. Metall. Mater.* **25** 2533
[24] Edwards J T and Thouless D J 1972 *J. Phys. C: Solid State Phys.* **5** 807
[25] Tsunetsugu H, Fujiwara T, Ueda K and Tokihiro T 1986 *J. Phys. Soc. Japan* **55** 1420
[26] Baake M, Kramer P, Schlottmann M and Zeidler D 1990 *Int. J. Mod. Phys.* B **4** 2217
[27] Grushko B 1992 *Phil. Mag. Lett.* **66** 151
[28] von Barth U and Hedin L J 1972 *J. Phys. C: Solid State Phys.* **5** 1629
[29a] Beer N and Pettifor D G 1984 *Electronic Structure of Complex Systems* ed P Phariseau and W M Temmerman (New York: Plenum) p 769
[29b] Allan G 1984 *J. Phys. C: Solid State Phys.* **17** 3954; 1985 *The Recursion Method and its Applications (Springer Series in Solid State Sciences 58)* ed D G Pettifor and D L Weare (Berlin: Springer)
[30] Bose S K, Winer K and Andersen O K 1988 *Phys. Rev.* B **37** 6262
Bose S K, Jaswal S S, Andersen O K and Hafner J 1988 *Phys. Rev.* B **37** 9955
Nowak H J, Andersen O K, Fujiwara T, Jepsen O and Vargas P 1991 *Phys. Rev.* B **44** 3577
[31] Bose S K, Ballentine L E and Hammerberg J E 1983 *J. Phys. F: Met. Phys.* **13** 2089
[32] Bose S K, Jepsen O and Andersen O K 1993 *Phys. Rev.* B **48** 4265
[33] Sluiter M and Varma C M 1981 *Phys. Rev.* B **23** 1633
[34] Pettifor D G and Varma C M 1979 *J. Phys. C: Solid State Phys.* **12** L253
[35] Niizeki K and Akamatsu T 1990 *J. Phys.: Condens. Matter* **2** 7043
[36] Niizeki K 1991 *J. Phys. A: Math. Gen.* **23** 4569; 1992 *J. Phys. A: Math. Gen.* **24** 1035
[37] Lück R and Kek S 1993 *J. Non-Cryst. Solids* **153–4** 329
[38] Sabiryanov R F and Bose S K 1994 *J. Phys.: Condens. Matter* **6** 6197; 1995 *J. Phys.: Condens. Matter* **7** 2375
[39] Ballentine L E and Hammerberg J E 1984 *Can. J. Phys.* **62** 692
[40] Vacancy-related disorder, not considered in this paper, may provide an additional contribution to the stability of these alloys at higher temperatures.